Fresnel hologram reconstruction of complex three-dimensional object based on compressive sensing

Xuemei Cao (曹雪梅)[1*], Xinzhu Sang (桑新柱)[1], Zhidong Chen (陈志东)[1], Ying Zhang (张 颖)[2], Junmin Leng (冷俊敏)[1], Nan Guo (郭 南)[1], Binbin Yan (颜玢玢)[1], Jinhui Yuan (苑金辉)[1], Kuiru Wang (王葵如)[1], and Chongxiu Yu (余重秀)[1]**

[1]*State Key Laboratory of Information Photonics and Optical Communications, Beijing University of Posts and Telecommunications (BUPT), Beijing 100876, China*

[2]*College of Science, Minzu University of China, Bejing 100081, China*

[*]*Corresponding author: xuemei_cao88@163.com;* [**]*corresponding author: xzsang@gmail.com*

Received February 28, 2014; accepted May 22, 2014; posted online July 18, 2014

Reconstruction the computer generated Fresnel hologram of complex 3D object based on compressive sensing (CS) is presented. The hologram is synthesized from a color image and the depth map of the 3D object. With the depth map, the intensity of the color image can be divided into multiple slices, which satisfy the condition of the sparsity of CS. Thus, the hologram can be reconstructed at different distances with corresponding scene focused using the CS method. The quality of the recovered images can be greatly improved compared with that from the back-propagation method. What's more, with the sub-sampled hologram, the image can be ideally reconstructed by the CS method, which can reduce the data-rate for transmission or storage.

OCIS codes: 090.1760, 090.2870.
doi: 10.3788/COL201412.080901.

As an alternative of Nyquist sampling theorem, the compressive sensing (CS) technology was presented in 2006[1−4]. Compared with the Nyquist sampling rate postulated by Shannon in 1949[5], the CS method is more effective to obtain and reconstruct the signal with a much lower sample rate. CS aims to minimize the redundant data collection, which can solve the problems of signal reconstruction under-sampling. There are two premises for the CS[6]. One is that the input signal or its transformation must be sparse. The other is that the sensing requirement can be expressed in terms of incoherence between the sampling operator and sparsity basis. CS technology has attracted considerable attentions. One of the fields that benefits from CS is compressive imaging[7,8]. Among them, phase estimation by the transport of intensity equation (TIE) based on CS has been reported[9].

Since digital holography satisfies the two premises of the CS, CS has been introduced[10,11]. The first premise is that the object can be transformed into scattering planes, which satisfies the sparsity of CS. The other one is that the holography measurement meets the condition of the incoherence measurements of CS, because light scattered from the object spreads out over many pixels on the hologram plane. Holography as a CS problem was suggested by Brady *et al.*[12]. Recently, many compressive holography applications have been discussed, such as compressive phase-shift Fresnel holography[13], compressive multiple view projection incoherent holography[14], off-axis frequency shifting holography[15], off-axis holography of diffuse objects[16], and multidimensional imaging compressive holography[17]. However, these previous reports aim to reconstruct the virtual 3D object consisting with simple flats by CS. The CS approach has not been applied to reconstruct a real complex 3D scene.

The object field distribution of the 3D object with complex structure is difficult to be described using a specific function. A large amount of information of the 3D object increases the difficulty to calculate the hologram. Computer generated hologram (CGH) technology is a combination of optical holography with computer technology, which can record and reconstruct vivid 3D scene of both virtual and real objects without a highly stable coherent optical system needed compared with the digital hologram[18,19]. It has been intensively investigated[20,21]. To synthesize the CGH, point-based[22,23] and mesh-based methods[24,25] were presented. The point-based method calculates the hologram pattern point-by-point, and then sums the patterns to produce the final hologram. Thus, a large amount of data is needed to ensure a better effect. One of the advantages of the point-based method is the adaptability to any 3D structure and its ability to provide a majority of the 3D visual cues. To accelerate the calculations, the mesh-based method is put forward. A number of triangles are used to compose a 3D scene. The holographic pattern of each triangle is calculated and then rotated to the corresponding position in the frequency domain. In our implementation of the CGH, the image-based method is used. The CGH is generated from a color image and the depth map with much less calculation amount compared with the point-based and the mesh-based method. Although the method provides fast calculation, it cannot provide view-dependent shading because the contents are intrinsically 2D images.

Inspired by the previous compressive works, reconstruction the CGH of complex 3D object synthesized from a color image and the depth map based on CS is proposed. The reconstructed results with the CS method are greatly improved compared with the conventional straightforward back-propagation method. In the recon-

struction results of the back-propagation method, the whole reconstruction image plane is distorted resulting in that the focused image cannot be recognized clearly. The reconstructed results of CS method show that different scenes corresponding to the object slices are clearly focused at different distances. What's more, even with part of the hologram data, the reconstructed focused images can be recognized.

The intensity of the color image of a complex 3D scene is divided into multiple slices based on the value of the depth map. Points with the same depth value are regarded as the same slice. The depth value of each slice is transformed into the distance of diffraction. According to the principle of tomography, the Fresnel hologram of the whole 3D scene can be achieved with the angular spectrum method (ASM)[26].

Figure 1 illustrates the schematic diagram of the CGH, in which the diffraction distance of each slice is decided by the value of the depth map. δ is the depth interval between the two neighboring object slices. $\mathrm{dep_{max}}$ and $\mathrm{dep_{min}}$ indicate the maximum and the minimum values in the depth map. The total slices of the 3D scene can be expressed as $n = \frac{\mathrm{dep_{max}} - \mathrm{dep_{min}}}{\delta}$. d_0 represents the distance of the farthest object plane between the hologram plane and d_i is the distance of ith object plane between the hologram plane. Then, $d_i = d_0 - i\delta$ can be obtained.

The diffraction field $D(x, y)$ of the 3D object is defined under the Born approximation as

$$D(x,y) = \iiint \mathrm{d}\varepsilon \mathrm{d}\eta \mathrm{d}z \beta(\varepsilon,\eta,z) h(x-\varepsilon, y-\eta, z), \quad (1)$$

where β is the scattering potential of a 3D object and h is the point spread function[27]. According to the ASM, the diffraction field $D_i(x, y; d)$ of the ith object plane $O(\xi, \eta; d_i)$ can be expressed as

$$D_i(x,y;d_i) = F^{-1}\left\{F\left[O(\xi,\eta;d_i)\right] \exp\left(\mathrm{i}2\pi d_i \sqrt{\frac{1}{\lambda} - f_x^2 - f_y^2}\right)\right\}, \quad (2)$$

where $\exp\left[\mathrm{i}2\pi d_i \sqrt{\frac{1}{\lambda} - f_x^2 - f_y^2}\right]$ is the transfer function, which is Fourier transformed from the point spread function. F and F^{-1} represent the Fourier transform and the inverse Fourier transform respectively.

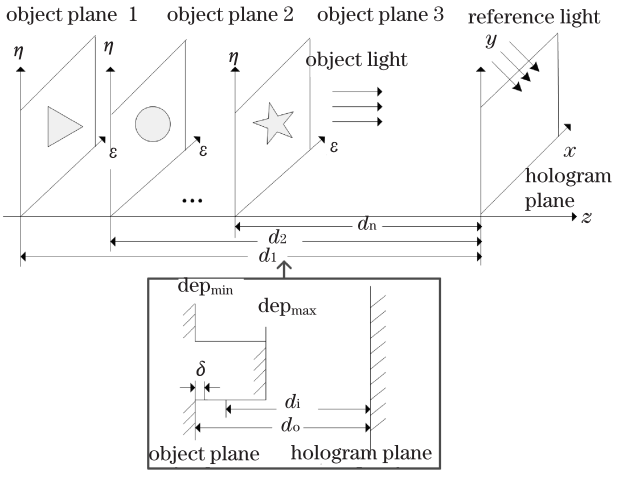

Fig. 1. Schematic diagram of the Fresnel CGH.

By adding the diffraction field of all the object planes, the whole 3D diffraction field $D(x, y)$ can be obtained

$$D(x,y) = \sum_{i=1}^{n} F^{-1}\left\{F\left[O(\xi,\eta;d_i)\right] \exp\left[\mathrm{i}2\pi d_i \sqrt{\frac{1}{\lambda} - f_x^2 - f_y^2}\right]\right\}. \quad (3)$$

To meet the linear mapping conditions of CS, the on-axial interferometry is employed. Assuming that the reference beam $R(x, y)$ is 1, the hologram $H(x, y)$ can be expressed as

$$\begin{aligned} H(x,y) &= |D(x,y) + R(x,y)|^2 \\ &= D(x,y) + D^*(x,y) + |D(x,y)|^2 \\ &= 2\mathrm{Re}\left[D(x,y)\right] + |D(x,y)|^2. \end{aligned} \quad (4)$$

In Eq. (4), $|D(x, y)|^2$ is regarded as the model error, which can be removed by eliminating the direct current (DC) term. Thus, the hologram measurement of Eq. (4) is a linear transformation between the object diffraction density and the measurement data. Then the diffraction field $D(x, y)$ and the hologram $H(x, y)$ can be expressed as a matrix-vector representation as

$$\mathbf{D} = \sum_{i=1}^{n} \mathbf{F}^{-1}\mathbf{Q}_i\mathbf{F}\mathbf{O}_i, \quad (5a)$$

$$\mathbf{H} = 2\mathrm{Re}\Big(\sum_{i=1}^{n} \mathbf{F}^{-1}\mathbf{Q}_i\mathbf{F}\mathbf{O}_i\Big) + c, \quad (5b)$$

where $\mathbf{F}$ represents the matrix form of the 2D disorete Fourier transform (DFT), and $\mathbf{F}^{-1}$ is the 2D inverse DFT matrix. The matrix $\mathbf{Q}_i$ is a diagonal matrix with appropriate quadratic phase elements along its diagonal. $\mathbf{O}_i$ is the ith object plane, which is a 1D vector obtained by rearranging the image in a lexicographic order. c is the constant term.

The reconstruction of different 2D images from a 2D hologram is an ill-posed inverse problem. CS offers mathematical reconstruction guarantees and supporting algorithmic frameworks for ill-posed inverse problems. Thus, the reconstruction of different object planes from the hologram can be formulated according to CS theory. It is a constrained optimization problem. The minimization of $\| \mathbf{O}_i \|_{\mathrm{TV}}$ tends to find a sparse solution, while the l_2 norm insures data consistency. τ is a regularization parameter, which controls the ratio between the data fit and the sparsity level. By solving, the object estimate is iteratively updated under sparse constraint on a total variation (TV) basis. The number of iterations is a critical parameter to stably converge to the solution.

$$\widetilde{O}_i = \arg\min_{O}\left\{\| \mathbf{H} - \mathbf{\Phi}\sum_{i=1}^{n}\varphi O_i \|_2^2 + \tau \| \mathbf{O}_i \|_{\mathrm{TV}}\right\}, \quad (6a)$$

$$\widetilde{O}_i = \arg\min_{O}\left\{\| \mathbf{H} - \mathbf{\Phi}\sum_{i=1}^{n}\mathbf{F}^{-1}\mathbf{Q}_i\mathbf{F}\mathbf{O}_i \|_2^2 + \tau \| \mathbf{O}_i \|_{\mathrm{TV}}\right\}, \quad (6b)$$

where $\| \cdot \|_p$ is the l_p-norm. $\mathbf{\Phi}$ is the a measurement matrix of the hologram domain. With a sampling percentage, it chooses M samples of the hologram to reconstruct the object plane. In order to satisfy the restricted

isometry property (RIP), which refers to that the measurement matrix $\mathbf{\Phi}$ should be incoherent with sensing matrix φ, the Gaussian random matrix is chosen as the measurement matrix $\mathbf{\Phi}$[28]. An operator (TV) which promotes the sparsest representation for the object plane O_i as stated in Ref. [12] is expressed as

$$\| \mathbf{O}_i \|_{\mathrm{TV}} = \sum_i \sum_{m,n} \sqrt{(\mathbf{O}_{m+1,n,i} - \mathbf{O}_{m,n,i})^2 + (\mathbf{O}_{m,n+1,i} - \mathbf{O}_{m,n,i})^2}. \quad (7)$$

which means that O_i is enforced by a sparsity constraint on the TV.

The two-step iterative shrinkage/thresholding (TwIST) algorithm[29] is employed to solve Eq. (6). It is an improved algorithm of the iterative shrinkage/thresholding (IST) algorithm to the convergence rate. To solve linear inversion problems, the algorithm minimizes an objective function with a nonquadratic regularizer such as TV. The objective function is regularized by the nonquadratic term to overcome the ill-conditioned nature of the linear transformation.

Figure 2 shows the color image and the depth map of a complex 3D scene, which are provided by the Middlebury stereo website. The depth map can also be obtained by the stereo matching technology[30]. The pixels of the two images are 374(H) × 374(V) and the pixel pitch is 30 μm. The hologram has the same pixels and the pixel pitch of the two images.

The wavelengths of the red, green, and blue light are $\lambda_{\mathrm{r}} = 625$ nm, $\lambda_{\mathrm{g}} = 532$ nm, and $\lambda_{\mathrm{b}} = 473$ nm respectively. According to the depth value of the depth map, $\mathrm{dep}_{\max} = 20.7$ mm, $\mathrm{dep}_{\min} = 0$. In order to shorten the calculation time and obtain the reconstruction image with more information focused at each slice, the depth interval is chosen as $\delta = 5.2$ mm. Then the whole 3D scene can be divided into four slices. However, the occlusion part is regarded as the farthest scene in the depth map, which is the error in the depth map. Thus, the 3D scene with depth values between 0 and 5.1 mm is neglected in our process. The points with 5.2 mm $\leqslant$ dep $\leqslant$ 10.3 mm, 10.4 mm $\leqslant$ dep $\leqslant$ 15.5 mm, and 15.6 mm $\leqslant$ dep $\leqslant$ 20.7 mm are regarded as the first, second, and third object slices respectively. Figure 3

Fig. 2. (Color online) (a) Color image and (b) depth image.

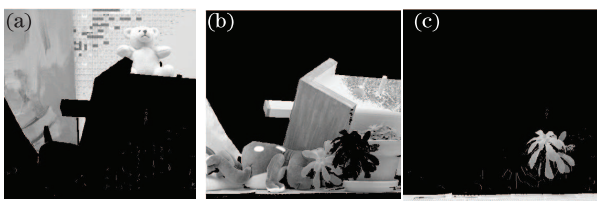

Fig. 3. Three objet slices.

(a) (b) (c)

Fig. 4. (Color online) Reconstructed images at distances of (a) d_1, (b) d_2, and (c) d_3 using the back-propagation method.

(a) (b) (c)

Fig. 5. (Color online) Reconstructed images at distances of (a) d_1, (b) d_2, and (c) d_3 using the CS method with 100%, 80%, 60%, and 40% of the hologram data.

shows the generated three objet slices. In the discretization of continuous depths into three depth planes, the points with different depth values among a certain range are assumed to be the same depth value, which causes depth errors in the reconstruction. However, the depth errors do not affect the verification of the successful reconstruction of the 3D scene. What's more, with the increase of the depth planes, the depth errors can be reduced. If the depth interval δ is controlled smaller than the vertical resolution of the human eyes, the depth errors can be neglected.

Supposing that the distance of the farthest object plane between the hologram plane is $d_0 = 500$ mm, then the distances of the three object slices between the hologramare $d_1 = 494.8$ mm, $d_2 = 489.6$ mm, and $d_3 = 484.4$ mm respectively. According to the synthetic method of the Fresnel hologram introduced, the Fresnel hologram can be obtained.

Figure 4 shows the reconstructed results using the back-propagation method of ASM. The focused images at different distances corresponding to the three object slices (in Fig. 3) cannot be recognized clearly. The appearing distortions are related to the model mismatch. The back-propagation follows a 2D-2D model (between the 2D depth plane to the 2D recording plane), therefore,

Table 1. PSNRs of Reconstructed Images

z (mm)	PSNR (dB)				
	Back Propagation Method	CS Method (Different Percents of the Hologram Data)			
		100%	8 0%	60%	40%
d_1	21.7758	28.7074	26.8504	23.7074	21.4287
d_2	22.9931	28.6632	26.2590	23.6549	20.6665
d_3	22.7058	28.4598	25.1709	23.0181	20.5149

points from other slices are numerically linked to the focused plane in the reconstruction process.

To estimate the reconstructed images by using the CS method, the computational procedure includes the following steps. Firstly, the superposition of the holograms from the three slices of the 3D scene achieves the final hologram. Then, with a sampling percentage, the Gaussian random matrix chooses M samples of the hologram. Thirdly, the parameters and the matrix operation needed in the TwIST algorithm are set. Finally, the TwIST algorithm is used to solve Eq. (6) to reconstruct the images. In our implementation, the number of iterations is set to be 500 and the regularization parameter τ is set to be 0.2.

Figure 5 shows the reconstructed images using the CS technology with sub-sampled hologram data. The first, second, third, and fourth rows in Fig. 5 represent that 100%, 80%, 60%, and 40% of the hologram data is used in reconstruction process respectively. Compared with Fig. 4, the reconstructed images corresponding to the three object slices (in Fig. 3) are in focus at different distances. The clear focused scenes can be obtained. What's more, even with 40% of the hologram information, the focused images can be recognized. Peak signal to noise ratio (PSNR) is used to evaluate the quality of the target area of the reconstruction images. The results are shown in Table 1, from which we can see that the reconstruction results by the CS scheme are superior to that of the back-propagation method.

In conclusion, a novel method to reconstruct the CGH of complex 3D scene based on CS is presented. The CGH is synthesized based on a color image and the depth map of the 3D scene. The results show that the CS reconstruction method can digitally focus on different 3D object planes of the hologram ideally, while the back-propagation method result in distortion in the reconstructed images. Moreover, with only part of the hologram information, the images can be reconstructed correctly.

This work was partly supported by the National Natural Science Foundation of China (No. 61177018), the National "863" Program of China (No. 2012AA011902), the Program for New Century Excellent Talents in University (No. NECT-11-0596), the Key Program of Beijing Science and Technology Plan (No. D121100004812001), and Beijing Nova Program (No. 2011066).

References

1. D. L. Donoho, IEEE Trans. Inform. Theory **52,** 1289 (2006).
2. E. J. Candès, J. K. Romberg, and T. Tao, Commun. Pure Appl. Math. **59,** 1207 (2006).
3. E. Candès and M. Wakin, IEEE Signal Process. Mag. **25,** 21 (2008).
4. A. M. Bruckstein, D. L. Donoho, and M. Elad, SIAM Rev. **51,** 34 (2009).
5. C. E. Shannon, Proc. IRE **37,** 10 (1949).
6. E. Candes and J. Romberg, Inverse Probl. **23,** 969 (2007).
7. M. F. Duarte, M. A. Davenport, D. Takhar, J. N. Laska, T. Sun, K. F. Kelly, and R. G. Baraniuk, IEEE Signal Process. Mag. **25,** 83 (2008).
8. J. Romberg, IEEE Signal Process. Mag. **25,** 14 (2008).
9. L. Tian, J. C. Petruccelli, Q. Miao, H. Kudrolli, V. Nagarkar, and G. Barbastathis, Opt. Lett. **38,** 3418 (2013).
10. Y. Rivenson, A. Stern, and B. Javidi, Appl. Opt. **52,** A423 (2013).
11. Y. Rivenson and A. Stern, Opt. Lett. **36,** 3365 (2011).
12. D. J. Brady, K. Choi, D. Marks, R. Horisaki, and S. Lim, Opt. Express **17,** 13040 (2009).
13. Y. Rivenson, A. Stern, and B. Javidi, J. Display Technol. **6,** 506 (2010).
14. Y. Rivenson, A. Stern, and J. Rosen, Opt. Express **19,** 6109 (2011).
15. M. M. Marim, M. Atlan, E. Angelini, and J. C. Olivo-Marin, Opt. Lett. **35,** 871 (2010).
16. K. Choi, R. Horisaki, J. Hahn, S. Lim, D. L.Marks, T. J. Schulz, and D. J. Brady, Appl. Opt. **49,** H1 (2010).
17. R. Horisaki, J. Tanida, A. Stern, and B. Javidi, Opt. Lett. **37,** 2013 (2012).
18. H. Ou, T.-C. Poon, K. K. Y. Wong, and E. Y. Lam, Photon. Res. **2,** 64 (2014).
19. A. Goy and D. Psaltis, Photon. Res. **1,** 96 (2013).
20. H. Shen, R. Zhu, Z. Gao, E. Y. B. PUN, W. H. Wong, and X. Zhu, Chin. Opt. Lett. **11,** 032201 (2013).
21. P. Tsang, K. W.-K Cheung, and T. C. Poon, Chin. Opt. Lett. **11,** 020901 (2013).
22. A. D. Stein, Z. Wang, and J. S. Leigh Jr., Comput. Phys. **6,** 389 (1992).
23. M. Lucente, J. Electron. Imaging **2,** 28 (1993).
24. H. Kim, J. Hahn, and B. Lee, Appl. Opt. **47,** D117 (2008).
25. J. Hong, Y. Kim, H.-J. Choi, J. Hahn, J.-H. Park, H. Kim, S.-W. Min, N. Chen, and B. Lee, Appl. Opt. **50,** H87 (2011).
26. J. W. Goodman, *Introduction to Fourier Optics* (Robert & Company, 2005) pp. 46-66.
27. D. J. Brady, *Optical Imaging and Spectroscopy* (Wiley, 2009).
28. E. Candès, J. Romberg, and T. Tao, IEEE Trans. Inf. Theory **52,** 489 (2006).
29. J. M. Bioucas-Dias and M. A. T. Figueiredo, IEEE Trans. Image Process. **16,** 2992 (2007).
30. H. Hirschmuller and D. Scharstein, in *Proceedings of IEEE Conference on Computer Vision and Pattern Recognition* 1 (2007).